NUMERICAL INVESTIGATION OF EFFECT OF THE FLOW FIELD STRUCTURE AND COOLING MEDIUM OF TUBES ON THE HEAT TRANSFER PERFORMANCE OF AUTOMOTIVE RADIATOR

by

Zongpeng MA, Ying HUANG*, XiaoLing CHEN, Jiangnan SONG, Xiang ZHANG, Taike LI, and Lunjun CHEN

School of Mechanical Engineering, Guizhou University,
Guiyang, Guizhou, China

Original scientific paper
https://doi.org/10.2298/TSCI221229118M

The flow field structure and cooling medium of tubes have major influence on the heat transfer performance of automotive radiator. In this study, two novel types of radiator tube (wasp-waisted tube 2# and wasp-waisted tube 3#) are developed, six types radiator tubes with different flow field structures and equal flow cross-sectional area are numerically simulated. In addition, four nanofluids with different concentrations (Al_2O_3-water, SiO_2-water, TiO_2-water, and CuO-water) were studied in Reynolds number 2500-7500. The results show that the heat transfer capacity of the wasp-waisted tube 2# and the wasp-waisted tube 3# is significantly better than that of the other radiator tubes, followed by the wasp-waisted tube. Compared with the wasp-waisted tube, the heat transfer coefficient of the wasp-waisted tube 2# and the wasp-waisted tube 3# increased by 10.6% and 3.5%, respectively. On the other hand, nanoparticles improve the heat transfer efficiency of base fluid. When Reynolds number reaches 7500 and the volume concentration is 3%, the Nu_{nf}/Nu_{bf} of SiO_2-water is 5.52%, 5.22%, and 8.70% higher than that of Al_2O_3-water, TiO_2-water, and CuO-water, respectively. The comprehensive heat transfer capacity of SiO_2-water-3% in the wasp-waisted tube is the best.

Key words*: wasp-waisted tube (radiator tube), CFD, flow field structure, heat transfer capacity (performance), nanofluid*

Introduction

Automobile radiator is an important part of automobile engine cooling system. It ensures that the engine is within the normal operating temperature range. Its heat transfer performance not only has great influence on the service life of automobile engine, but also indirectly affects the stability of automobile operation. The fin-and-tube radiator has good heat transfer performance and manufacturing process, and is a commonly used automobile radiator. As modern society demands more energy saving and consumption reduction, improving the heat transfer efficiency and reducing the volume of automobile radiator has become the focus of researchers. At present, there are two methods to solve this problem: active method

*Corresponding author, e-mail: huangydxy@163.com

and passive method. Active methods use external force or equipment to improve heat transfer performance, which increases cost and energy consumption to a certain extent. The passive method is realized by changing the flow field structure in the radiator tube or changing the thermophysical properties of the cooling medium [1, 2].

Numerous studies have been done on the performance of radiators, particularly radiator tubes [3-7]. Hussein *et al*. [8] numerically studied the heat dissipation and resistance properties of three nano-fluids in three kinds of tubes by analyzing pressure drop, temperature distribution, Nusselt number, and its sensitivity. In the comparison between the elliptic tube and the circular tube, the elliptic tube has better heat transfer capacity and greater pressure drop. Tala *et al*. [9] studied the effects of changes in the shape of equal-section tubes (from circular to elliptical) on the heat dissipation characteristics and the entropic yield on the air side under three radiator tube shapes and two air velocities. It was found that the thermal and viscous entropies decreases significantly when the tube with equal section changes from circular to elliptical. The equal-section elliptical tube heat exchanger has a thermal-hydraulic performance that is 80% better than the traditional circular finned tube heat exchanger. In addition, the researchers found that heat transfer efficiency could be improved by placing spoilers in the tubes. Chiam *et al*. [10] analyzed heat tube of different structures. It is proved that the inserts can effectively increase the heat transfer capacity of the tubes.

According to the research, radiator tube heat transfer performance can be further enhanced by changing the flow field structure of the radiator tube. However, at present, there are few studies in the flow field structure of new tubes, especially tubes with special flow field structures, which should be further studied through experiments or numerical simulations. In addition, in order to further enhance the heat transfer performance of the radiator, some studies have used nanofluids as the cooling medium of the radiator to further enhance the heat transfer capability. Nanofluids are a new type of fluids which disperse metal or non-metal nanoparticles (1-100 nm) in basic liquids such as water, glycol and glycerin. Because metals generally have better thermal conductivity than liquids, metal particles are dispersed in liquids and, due to Brownian motion, can theoretically improve their thermal conductivity [11-16]. Zhao *et al*. [17] quantitatively studied the heat dissipation performance of nano-fluid (Al_2O_3-water) in a flat tube. The effects of Reynolds number, concentration, particle size and other characteristics of nanofluids were analyzed. The results show that the nanofluid has better heat transfer ability than the base fluid. Manca *et al*. [18] studied the distribution form of required pumping power and the heat transfer coefficient of nano-fluid in the 2-D channel, and concluded that the heat transfer capacity of nanofluid is proportional to the concentration of nanofluid, but the required pumping power is also increasing. Namburu *et al*. [19] studied the particle size of nanoparticles, and the particle size of nanoparticles is inversely proportional to Nusselt number. The study of AlO, SiO, and CuO nanoparticles found that when the CuO concentration was 6%, the Nusselt number of nanofluids increased by 35%. Mohammed *et al*. [20] studied the flow properties and thermophysical properties of nanofluids in circular tubes with tapered ring inserts. Four nanofluids with diameters of 20~50 nm were selected to prepare nanofluids with concentrations of 1~4%. The effects of different Reynolds numbers and tapered ring types are investigated. The results demonstrated that SiO_2-water nanofluids perform better in terms of heat transmission and have reduced resistance. Nusselt number is proportional to concentration and Reynolds number and inversely proportional to nanoparticle diameter. Kumar *et al*. [21] studied the effect of heat transfer in tubes on the thermophysical properties of Al and Cu oxide-based nanofluids. Compared with the 162% increase in Al_2O_3-based nanofluids, the Nusselt number of CuO-based nanofluids increased by 174%. Kumar *et*

al. [22] studies found that CuO/SiO_2 nanoparticles exhibit higher thermal conductivity. The increase in thermal conductivity of nanofluids is 6.5% higher than that of water/EG coolants. Nusselt number and heat transfer rate increased significantly by 48.24%.

In order to improve the radiation performance of automotive radiators, the cooling flow field and cooling medium of radiator tubes are studied in this study. In terms of cooling flow field of radiator tube, based on the existing wasp-waisted tube, this study designed wasp-waisted tube 2# and wasp-waisted tube 3#. According to the actual length of radiator tube, the relevant two-phase heat transfer model was established, and compared the performance of the two new radiator tubes with that of traditional radiator tubes (circular tube, elliptical tube, flat pipe, wasp-waisted tube). In terms of cooling medium of radiator tube, three kinds of metal particle nanofluids (Al_2O_3-water, TiO_2-water, and CuO-water) and one kind of non-metal particle nanofluids (SiO_2-water) were studied by using the wasp-waisted tube. Nussel number and resistance coefficient of nanofluids with different concentration in the tube were also studied. The optimal type and concentration of nanofluids in the wasp-waisted tube can be obtained by comparing the comprehensive heat transfer capabilities.

Materials and methods

Theoretical analysis

Figure 1(a) shows the radiator tubes used in this study, which are circular tube, elliptical tube, flat tube, wasp-waisted tube, wasp-waisted tube 2# and wasp-waisted tube 3#. On the basis of the wasp-waisted tube, the wasp-waisted tube 2# is fitted with two aluminum twist belts in the tube, and the wasp-waisted tube 3# enhances the degree of the waist collection. Figure 1(b) is the schematic heat transfer structure illustrating. The cooling medium enters the tube from the inlet and is discharged from the outlet, while the air flows from the outside of the tube. Table 1 lists the geometry of all tubes.

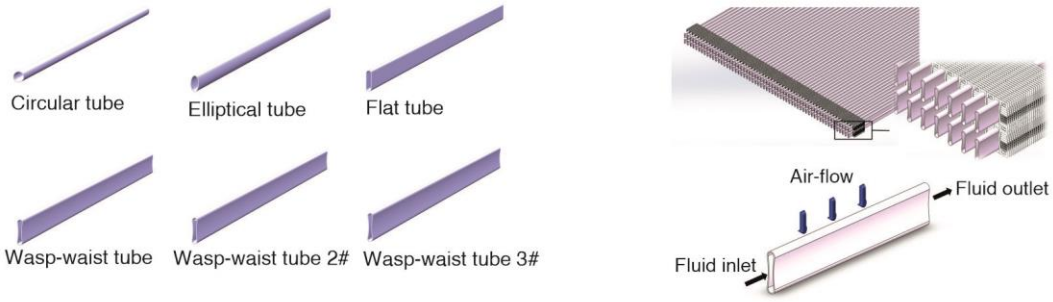

Figure 1. Problem geometry; (a) radiator tubes with different flow field structures and (b) schematic of the wasp-waisted tube heat transfer structure

Table 1. Geometric dimensions of all radiator tubes

Type	Cross sectional area [mm^2]	Hydraulic diameter [mm]
Circular tube	11.23	3.78
Elliptical tube	11.23	3.42
Flat tube	11.23	2.74
Wasp-waisted tube	11.23	2.23
Wasp-waisted tube 2#	11.23	2.23
Wasp-waisted tube 3#	11.23	2.03

Governing equations and boundary conditions

In this study, it is assumed that the fluid has uniform axial velocity and temperature at the inlet of the tube. Dispersions of low volume concentration nanoparticles in basic fluids can be treated as single phase fluids. Basic fluids and nanofluids are incompressible and compressive power and viscous dissipation is generally considered negligible for fluid flow inside a radiator. Under these conditions, the governing equations for turbulent mean continuity, momentum, and thermal energy are presented [23]:

Continuity equation:

$$(\nabla \bar{V}) = 0 \tag{1}$$

Momentum equation:

$$\rho(\nabla \bar{V})\bar{V} = -\nabla \bar{P} + \mu(\nabla^2 \bar{V}) - \rho(\nabla \overline{V'V'}) \tag{2}$$

Energy equation:

$$\rho C_p(\nabla \bar{V})\bar{T} = k(\nabla^2 \bar{V}) - \rho C_p(\nabla \overline{V'T'}) \tag{3}$$

where V' and T' are turbulent fluctuations and $\bar{V}, \bar{P}, \bar{T}$ are the time averaged mean values.

The k-ε model is used for the calculation and analysis in this paper. The model uses the following additional transfer equations for the dissipation rates of turbulent and turbulent energy:

$$\frac{\partial}{\partial x_i}\left(\rho\kappa\overline{u_i}\right) = \frac{\partial}{\partial x_i}\left[\left(\mu + \frac{\mu_t}{\sigma_\kappa}\right)\frac{\partial \kappa}{\partial x_j}\right] + \mu_t \frac{\partial \overline{u_i}}{\partial x_j}\left(\frac{\partial \overline{u_i}}{\partial \overline{x_j}} + \frac{\partial \overline{u_j}}{\partial \overline{x_i}}\right) - \rho\varepsilon \tag{4}$$

$$\frac{\partial}{\partial x_i}\left(\rho\varepsilon\overline{u_i}\right) = \frac{\partial}{\partial x_j}\left[\left(\mu + \frac{\mu_t}{\sigma_\varepsilon}\right)\frac{\partial \varepsilon}{\partial x_j}\right] + C_{1\varepsilon}\mu_t \frac{\varepsilon}{\kappa}\frac{\partial \overline{u_i}}{\partial x_j}\left(\frac{\partial \overline{u_i}}{\partial \overline{x_j}} + \frac{\partial \overline{u_j}}{\partial \overline{x_i}}\right) - C_{2\varepsilon}\rho\frac{\varepsilon^2}{\kappa} \tag{5}$$

where σ_κ and σ_ε are the effective Prandtl numbers that relate turbulent kinetic energy, κ, and rate of dissipation of turbulent energy, ε, respectively, to the momentum eddy viscosity, μ_t. The eddy viscosity is given as:

$$\mu_t = \frac{C_\mu \rho \kappa^2}{\varepsilon} \tag{6}$$

The eqs. (4)-(6), contain five adjustable constants: σ_κ = 1.00, σ_ε = 1.30, $C_{1\varepsilon}$ = 1.44, $C_{2\varepsilon}$ = 1.92, and C_μ = 0.09.

In this study, the flow characteristics of six different flow structures and four different volume concentration nanofluids were numerically analyzed, and turbulent viscous k-values were used at high Reynolds numbers. The k-ε Models (Re = 2500-7500) are used to study the heat transfer properties. In the numerical simulation of all tubes, the interface between tube and fluid is coupled boundary condition; on the other hand, pressure outlet boundary condition and velocity inlet boundary condition are adopted. The governing equations are solved using the controlled volume method of FLUENT 2020. Use the convection term, diffusion term, *etc*. of the second-order upwind discrete governing equation. Use SIMPLE format to handle pressure-velocity coupling. All calculations are performed with the double precision option. To solve linear systems produced by discretization, FLUENT combines the format of the algebraic multigrid approach with a point-implicit (Gauss-Seidel) linear equation solver. Convergent solutions are considered when the iterative processes of all governing equations produce normalized residuals.

The specific boundary conditions are set:

- *Inlet boundary conditions*: The water area in the tube and the air area outside the tube are both set as velocity inlet boundary conditions. The air inlet temperature is set to 293 K and the velocity is fixed at 8 m/s. The inlet temperature of liquid coolant is set at 353 K. The inlet velocity is calculated and set according to Reynolds number operating conditions.
- *Outlet boundary conditions*: The outlet conditions are set as pressure outlet boundary conditions, which are a standard atmospheric pressure.
- *Solid wall boundary conditions*: The inner wall of the tube is set as the coupled heat transfer surface, while the remaining surfaces are set as the wall boundary conditions.

Thermophysical properties of nanofluids

In this study, nanofluids are usually prepared by dispersing metallic nanoparticles or non-metallic nanoparticles into water. CuO-water, Al_2O_3-water, TiO_2-water, and SiO_2-water with different volume concentrations (0.5%, 1.0%, 2.0%, and 3.0%) were examined for their heat transfer properties. The single-phase approach can be employed if the particle distribution is fairly homogeneous and the nanoparticle diameter is very tiny [24]. The influence of temperature on the thermophysical properties of the mixture was considered. The following equations are used to determine thermal physical characteristics of nanofluids [25-27].

Density:

$$\rho_{\mathrm{nf}} = \varphi\rho_p + (1-\varphi)\rho_{\mathrm{bf}} \tag{7}$$

Specific heat:

$$C_{p,\mathrm{nf}} = \varphi\rho_p C_{p,p} + (1-\varphi)\rho_{\mathrm{bf}} C_{p,\mathrm{bf}}\rho_{\mathrm{nf}} \tag{8}$$

Thermal conductivity:

$$k_{\mathrm{nf}} = \left[\frac{k_p + 2k_{\mathrm{bf}} + 2(k_p - k_{\mathrm{bf}})(1+\beta)^3\varphi}{k_p + 2k_{\mathrm{bf}} - 2(k_p - k_{\mathrm{bf}})(1+\beta)^3\varphi}\right]k_{\mathrm{bf}} \tag{9}$$

Dynamic viscosity:

$$\mu_{\mathrm{nf}} = (1 + 7.3\varphi + 123\varphi^2)\mu_{\mathrm{bf}} \tag{10}$$

where β (β = 0.1) is the ratio of the nanolayer thickness to the original particle radius, φ – the nanoparticles volume concentration, and the subscripts nf, bf, and p refer to nanofluid, base fluid, and particle, respectively. The properties used in this study are listed in tab. 2.

Table 2. Thermal properties of nanoparticles

Nanoparticle	Density, [kgm^{-3}]	Specific heat, [Jkg^{-1}K^{-1}]	Thermal conductivity, [Wm^{-1}K^{-1}]	Reference
CuO	6000	551	33	[2]
Al_2O_3	3960	773	40	[28]
SiO_2	2220	745	1.4	[29]
TiO_2	4175	692	8.4	[30]

Data reduction

The calculation for the convective heat transfer coefficient is presented:

$$h_{\mathrm{nf}} = \frac{m_v C_p \rho_{\mathrm{nf}} (T_{\mathrm{in}} - T_{\mathrm{out}})}{S(T_{\mathrm{a}} - T_w)} \tag{11}$$

where S [m^2] is the inner wall area of the radiator tube and T_{in} and T_{out} represents the inlet and outlet temperature of the heat dissipation tube respectively.

The pressure drop in the radiator is computed using:

$$\Delta P = P_{in} - P_{out} \tag{12}$$

Equation (10) is used to calculate the Nusselt number:

$$\mathrm{Nu} = \frac{h_{nf} D_h}{k_{nf}} \tag{13}$$

where D_h is the hydraulic diameter of the radiator tube and k_{nf} is the thermal conductivity of nanofluids:

$$D_h = \frac{4A}{L} \tag{14}$$

where A represents the cross-sectional area of the radiator tube and L is the cross-sectional perimeter

The Reynolds number is obtained from:

$$\mathrm{Re}_{D_h} = \frac{\rho_{nf} v D_h}{\mu} \tag{15}$$

The friction factor is obtained from:

$$f = \frac{2 D_h \Delta P}{\rho_{nf} u^2 L} \tag{16}$$

The heat transfer performance cannot be simply considered and negative effects such as pressure drop or flow resistance in the tube should also be comprehensively considered in practical engineering. The detailed evaluation of the comprehensive thermal performance of nanofluids was done using the performance measurement evaluation method [10]. Under the Reynolds number conditions simulated in this study, the PEC comprehensive evaluation index is greater than 1 after the addition of nanoparticles, indicating that the addition of nanoparticles is conducive to improving the comprehensive heat transfer performance. The larger the PEC, the better the enhanced heat transfer effect. The PEC comprehensive evaluation index is less than 1, indicating that the addition of nanoparticles is not conducive to the improvement of comprehensive heat transfer performance. Equation (17) is used to calculate the PEC value:

$$\eta = \left(\frac{\mathrm{Nu}_{nf}}{\mathrm{Nu}_{bf}} \right) / \left(\frac{f_{nf}}{f_{bf}} \right)^{\frac{1}{3}} \tag{17}$$

Grid independence verification and experimental verification

In this paper, four kinds of meshes with different numbers were studied. Table 3 presents the pressure drop and temperature values applicable to different grids. When the number of grids of the calculation model reaches 3764096, the deviation is within the allowable range of calculation accuracy, and the average deviation of the pressure drop and temperature values is less than 0.4% and 0.1%, respectively. At this point, the further improvement of mesh number does not significantly improve the accuracy, various models with a grid number of 3764096 were selected for simulation. Data from the simulation and those from Fotukian and Esfahany [31] were compared in order to assess the simulation's accuracy. The results of the simulation analysis are in agreement with the experimental results, as shown in fig. 2, with a maximum deviation of 8.4%.

Table 3. Grid independence study

Groups	Grid number	ΔP [Pa]	T [K]
1	2873310	3406.904	338.4556
2	3332884	3579.713	338.2667
3	3764096	3643.961	338.0447
4	4180187	3655.799	338.046

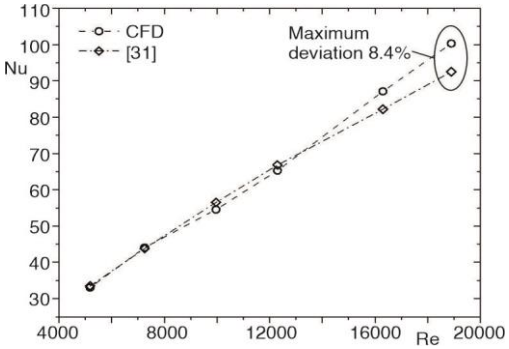

Figure 2. Model validation

Results and discussions

Effect of the flow field in the tube

Figure 3 displays the temperature contours for the six tubes in the longitudinal section under the same flow. Tubes with different flow field structures have significantly different outlet temperatures. Wasp-waisted tube has the lower outlet temperature than circular tube, elliptical tube, and flat tube, while wasp-waisted tube 2# and wasp-waisted tube 3# have a lower outlet temperature than wasp-waisted tube. Figure 4 shows the contour lines of the temperature of each tube on the cross section at the same position, the high temperature area of the waist tube is obviously smaller in the four tube types on the left. Compared with the wasp-waisted tube, the high temperature area of the wasp-waisted tube 3# is further reduced. The change in cross-sectional shape will affect the contact area between fluid and tube wall. Circular, elliptic, and flat tube types have hydraulic diameters that gradually get increasingly smaller. The wasp-waisted tube's hydraulic diameter is further decreased, and the wasp-waisted tube 3# has the smallest hydraulic diameter by strengthening the waist. Under the same flow rate and area, the smaller the hydraulic diameter of the tube, the larger the heat exchange area that the fluid in the tube contacts the inner wall when flowing. The wasp-waisted tube 2# 's improved heat transfer performance is caused by the inclusion of two twisted belts that increase the fluid's turbulence intensity and destroy the boundary layer, further enhancing the heat transfer performance. The figures demonstrate that compared with the wasp-waisted tube, the delamination of wasp-waisted tube 2# is not obvious, and the area of the high temperature area is smaller.

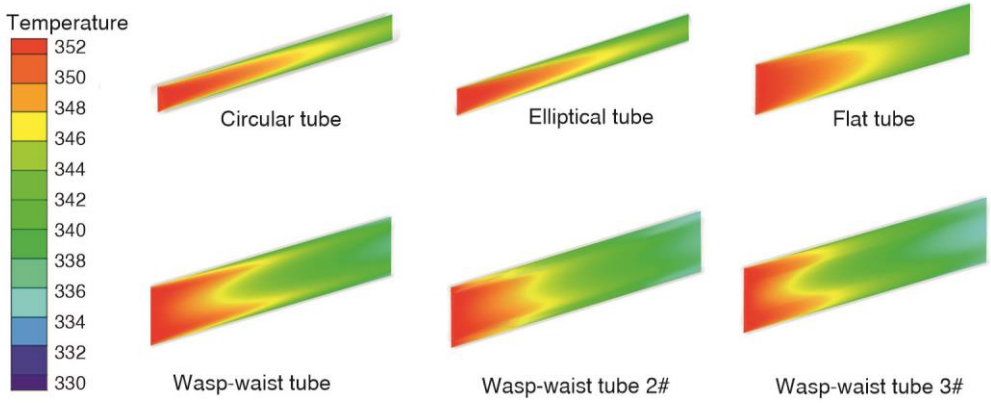

Figure 3. Temperature contours for the six tubes in the longitudinal section

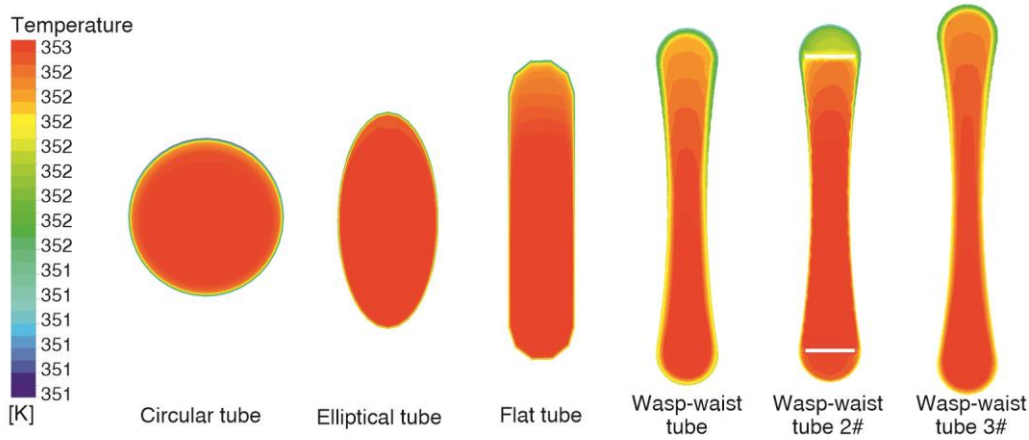

Figure 4. Temperature contours of the six tubes on the cross section at the same position

Numerical simulations were performed at six Reynolds numbers from 2500 to 7500 (step size 1000). The influence of different tube flow field structure and Reynolds number variation on fluid flow characteristics is analyzed. Figure 5(a) shows the convective heat transfer coefficient of each tube, and fig. 5(b) shows the pressure drop in each tube. With an increase in Reynolds numbers, the pressure drop and convective heat transfer coefficient rise, in the case of the same Reynolds numbers, the circular tube has a slightly lower heat transfer coefficient than elliptical tube. Compared with the two kinds of tubes, the heat transfer coefficient of the flat tube is greatly improved. But the heat transfer coefficient of the three tubes (circular tube, elliptical tube, and flat tube) is smaller than the wasp-waisted tube. When the Reynolds numbers reaches 7500, the heat transfer coefficient of the wasp-waisted tube increases by 66.3%, 45.6%, and 23.5%, respectively, compared with the circular tube, elliptical tube and flat tube. The two new tube types based on the wasp-waisted tube have enhanced heat transfer performance than the wasp-waisted tube. When the Reynolds numbers reaches 7500, the heat transfer coefficient of wasp-waisted tube 2# and wasp-waisted tube 3# increases by 10.6% and 3.5% compared with that of wasp-waisted tube, while the pressure increased

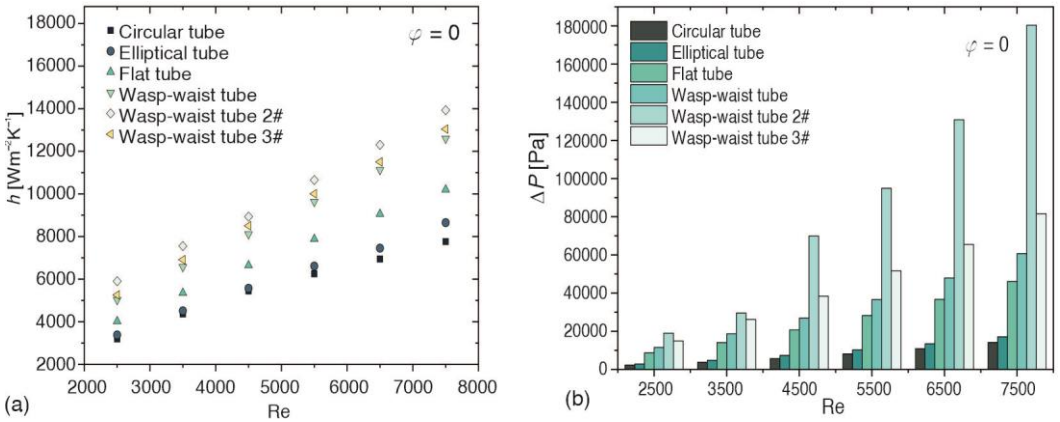

Figure 5. Fluid-flow properties in tubes with different flow field structures;
(a) variation of fluid-flow heat transfer coefficient with Reynolds numbers in tubes and
(b) variation of pressure drop with Reynolds numbers in tubes

157.3% and 34.3%, respectively. The results of six comparisons of circular tube, elliptical tube, flat tube, wasp-waisted tube, wasp-waisted tube 2#, and wasp-waisted tube 3# show that changing the fluid flow shape under the condition of equal section enhances the heat transfer coefficient of the fluid, but the pressure drop inevitably increases. The maximum heat transfer coefficient and highest pressure drop are found in wasp-waisted tube 2#.

The change of flow field structure not only affects the flow pattern of the fluid in the tube, but also changes the air flow shape outside the tube. Figure 6(a) illustrates the flow velocity around the tube at the same inlet velocity. It is clear that the air velocity is greatest around the circular tube, second by the elliptical tube, and then the flat tube. As the shape of the tube changes, the wasp waist tube further slows the air around it. The air velocity of wasp-waisted tube 3# in the windward is slightly higher than that of wasp-waisted tube. When the air velocity outside the tube is too high, inadequate heat exchange between air and the outer wall of the tube, and the heat transfer efficiency is reduced. The illustration shows that in the wasp-waisted tube, wasp-waisted tube 2# and wasp-waisted tube 3#, the air velocity decreases as it passes through the wasp-waisted area, and through observing the comparison results between the wasp-waisted tube and the wasp-waisted tube 3#, enhancing the degree of waist retraction can further reduce the air velocity in this area. In the process of heat exchange, the air inevitably produces gas vortex behind the tube, which will increase the air resistance and

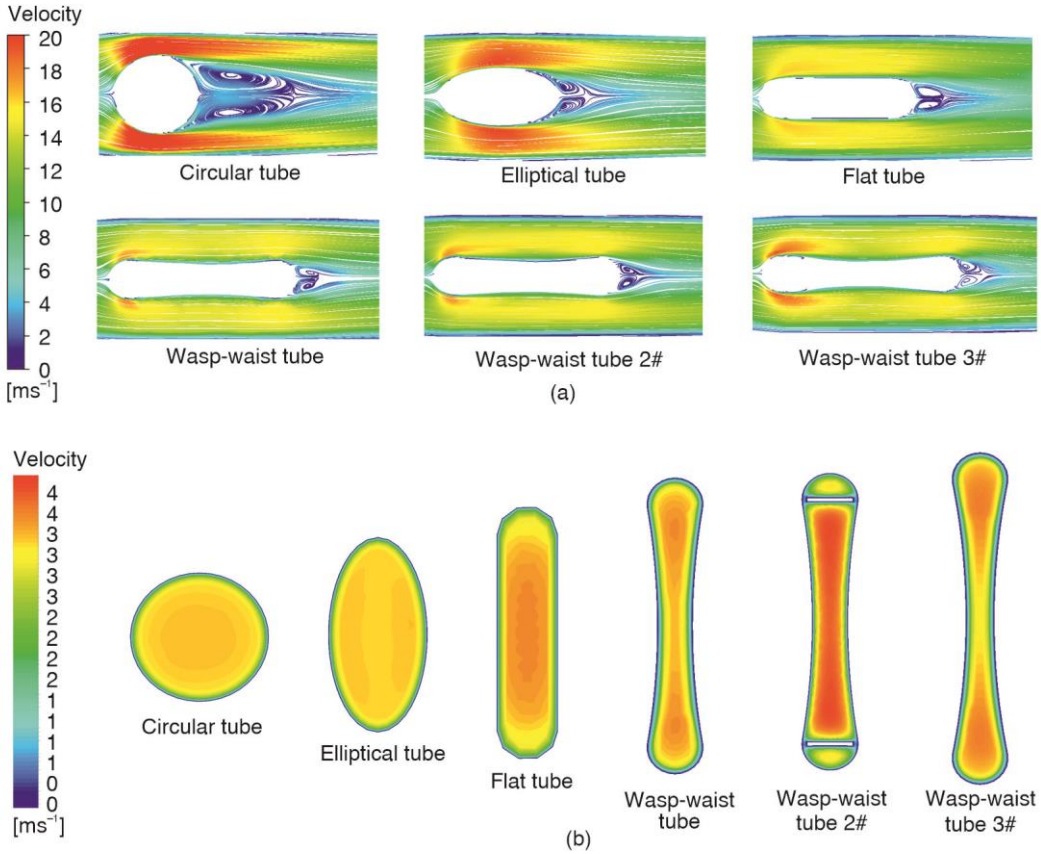

Figure 6. Velocity contours around tubes with different flow field structures; (a) air flow outside the tube and (b) coolant flow in the tube

the energy consumption of the radiator to a certain extent. The vortex area of circular tube is the largest, followed by elliptical tube, flat tube, wasp-waisted tube, wasp-waisted tube 2# and wasp-waisted tube 3#. With the change of tube shape more in line with the air flow direction, the air vortex decreases significantly. The wasp-waisted tube and wasp-waisted tube 2# have the same vortex area due to they have the same aerodynamic shape, the vortex area of the wasp-waisted tube 3# is similar to that of the wasp-waisted tube, but the strength is reduced. Under the same inlet velocity in the tube, the flow state in the radiator tube with different flow field structures differs greatly. Figure 6(b) shows the velocity profiles of cross sections in different tubes at the same position, with the lowest average velocity in a circular tube, followed by an elliptical tube and a flat tube. The wasp-waisted tube, wasp-waisted tube 2# and wasp-waisted tube 3# have generally higher fluid velocity inside the tube, which is due to the fact that the waisted shape will reduce the hydraulic diameter of the radiator tube while ensuring the same cross-sectional area, and this shape will increase the fluid pressure drop inside the tube and the fluid velocity, meanwhile, the wasp-waisted tube 2# will further aggravate this effect due to the setting of the twisted belt in it.

Influence of cooling medium

Figure 7 demonstrates that the variation of Nu_{nf}/Nu_{bf} of nanofluids with different concentrations (0.5%, 1.0%, 2.0%, and 3.0%) in the wasp-waisted tube at $2500 \leq Re \leq 7500$. According to the results, nanofluids perform better at heat transfer rate as concentration rises, while Reynolds number has little of an impact. At the specific Reynolds numbers, there is a large difference in Nu_{nf}/Nu_{bf} between different kinds of nanofluids with the same concentration. In metal particle nanofluids, TiO_2-water performed better in terms of heat transfer than the other two metal particle nanofluids. When Reynolds numbers reaches 7500 and the volume concentration is 3%, the Nu_{nf}/Nu_{bf} of TiO_2-water is 3.31% and 2.92% higher than that of CuO-water and Al_2O_3-water, respectively. The heat transfer capacity of metal particle nanofluid of each concentration is lower than that of non-metal particle nanofluid SiO_2-water. When Re = 7500 and the volume concentration is 3%, the Nu_{nf}/Nu_{bf} of SiO_2-water is 8.70%, 5.52%, and 5.22% higher than that of CuO-water, Al_2O_3-water and TiO_2-water, respectively.

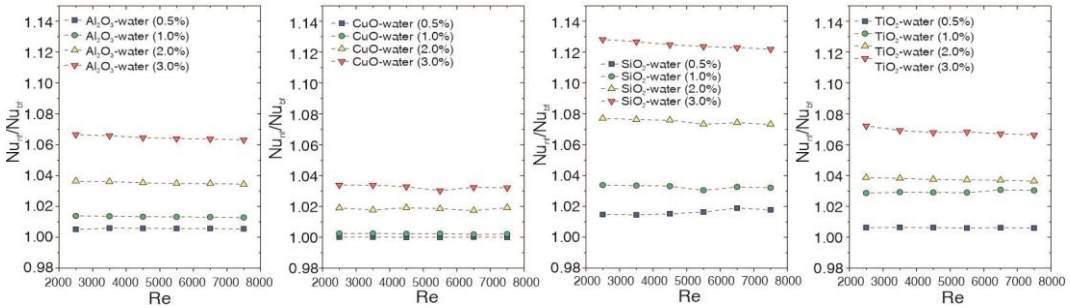

Figure 7. Comparison of Nu_{nf}/Nu_{bf} of different kinds and concentrations of nanofluids at specific Reynolds numbers

Although they enhance heat transfer efficiency, nanoparticles also make a fluid more viscous. Figure 8 depicts the impact of nanofluid concentration at the same inlet velocity on midline velocity. Due to the special structure of the wasp-waisted tube, the midline velocity reaches the peak at the geometric center of the circle at both ends and decreases at the wasp-waisted. Al_2O_3 and water flow at different concentrations have similar velocities close to the

wall, the midline velocity rises as the concentration of the nanofluid increases, and the difference is greater near the geometric center at both ends of the wasp-waisted tube. The results shown in fig. 8 indicated that that when the inlet velocity is the same, the nanofluid with higher concentration needs greater flow velocity in the tube. In addition, the friction coefficient of various nanofluids in fig. 9 is proportional to the concentration of nanofluids and inversely proportional to Reynolds numbers. With an increase in concentration, the SiO_2 nanofluid's friction coefficient slightly rises. When the Reynolds numbers reaches 7500, it increases by 1.0%, 1.7%, 2.9%, and 4.1%, respectively. The Al_2O_3-water and TiO_2-water have similar friction coefficient increases, both smaller than CuO-water. The CuO-water increased by 2.9%, 5.4%, 10.6%, and 15.5%, respectively, with the largest increase. On the other hand, the increase of the coefficient of friction of the fluid in the tube increases the fluid pressure drop of the overall radiator, which increases the pumping power of the radiator, and the higher the concentration of nanofluids, the greater the pumping power burden of the overall radiator.

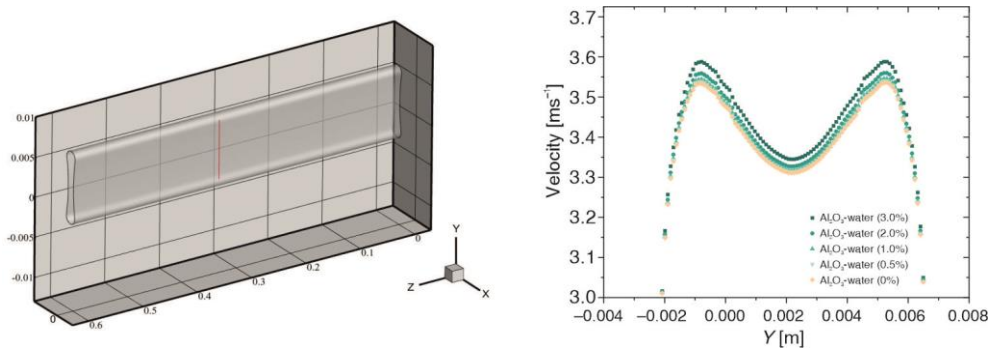

Figure 8. Comparison of midline velocities of nanofluids with different concentrations (Al_2O_3-water)

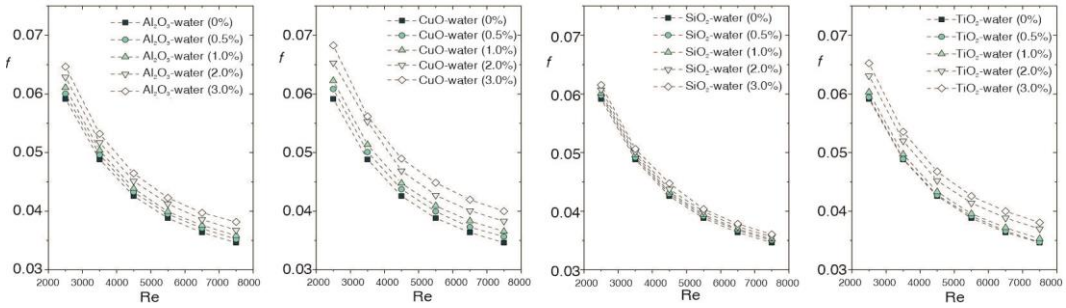

Figure 9. Comparison of friction coefficients of different kinds and concentrations of nanofluids at specific Reynolds numbers

Research was conducted on the flow resistance and heat transfer properties of nanofluids, respectively, but in practical engineering, the performance of cooling medium should be evaluated comprehensively. To verify the comprehensive heat transfer performance of nanofluids, a comprehensive evaluation factor based on liquid water is introduced in this study. Figure 10 shows the comprehensive evaluation of nanofluids with different concentrations. Generally, the evaluation standard of the comprehensive evaluation factor is to see whether its value is greater than 1. When the value is greater than 1, the addition of nanoparticles enhances the comprehensive heat transfer capacity of the base liquid. The PEC comprehensive evaluation indexes of SiO_2-water, Al_2O_3-water and

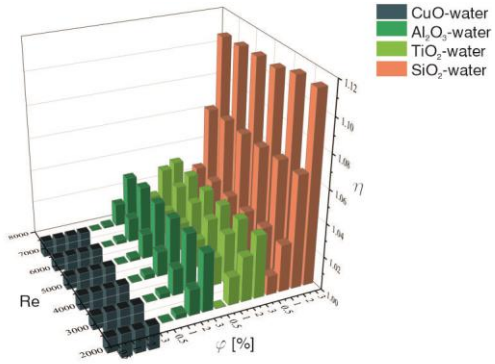

Figure 10. The PEC of nanofluids of different types and concentrations

TiO_2-water are all greater than 1 and increase with the concentration increases. The comprehensive performance of SiO_2-water with mass fraction of 3% is the best. The figures demonstrate that the comprehensive performance evaluation indexes of CuO-water are less than 1, indicating that the use of 0.5-3.0% mass fraction CuO-water nanofluid in the wasp-waisted tube cannot offset the increase of friction coefficient compared with the base fluid water.

Conclusions

In the study, six numerical models of equal flow cross-sectional area radiator tubes are investigated, tubes with different flow field structures were studied by two-phase flow and the influence of flow field structure changes on hydrothermal characteristics was analyzed. In the wasp-waisted tube, four nanofluids were studied, and the comprehensive performance evaluation indexes of nanofluids with different concentrations under specific Reynolds number were analyzed. The following conclusions are made based on the results of this study.

- The comparison results of five models including circular tube, elliptical tube, flat tube, wasp-waisted tube and wasp-waisted tube 3# show that changing the cross-section shape of fluid-flow in the case of equal cross-section significantly improves the convective heat transfer coefficient of fluid, and the convective heat transfer coefficient of radiator tube with equal cross-section increases with the decrease of hydraulic diameter. Due to its smaller hydraulic diameter and better aerodynamic shape, the heat transfer coefficient of wasp-waisted tube increases by 66.3%, 45.6%, and 23.5%, respectively, compared with circular tube, elliptical tube and flat tube. The heat transfer performance of the wasp-waisted tube 3# is better than that of the wasp-waisted tube. When the Reynolds numbers reaches 7500, the heat transfer coefficient of wasp-waisted tube 3# increases by 3.5%.
- In the case of the equal flow cross-sectional area, the addition of twisted tape in the wasp-waisted tube can further enhance the turbulence intensity and the convective heat transfer coefficient in the wasp-waisted tube, but the pressure drop is significantly increased at the same time. When the Reynolds number reaches 7500, compared with the wasp-waisted tube, the heat transfer coefficient of the wasp-waisted tube 2# is increased by 10.6%.
- In the wasp-waisted tube, both the flow resistance coefficient and the heat transfer coefficient of the nanofluid are enhanced with the increase of the concentration of the nanofluid. At the same concentration, the heat transfer performance of non-metallic particle nanofluids (SiO_2-water) is better than that of metal particle nanofluids (Al^2O^3-water, CuO-water, and TiO^2/water). When Reynolds numbers reaches 7500 and the volume concentration is 3%, the Nu_{nf}/Nu_{bf} of SiO_2-water is 8.70%, 5.52%, and 5.22% higher than that of CuO-water , Al_2O_3-water and TiO_2-water, respectively.
- The PEC comprehensive evaluation index is used to evaluate various nanofluids in the wasp-waisted tube, SiO_2-water, Al_2O_3-water, and TiO_2-water can improve heat transfer at a certain volume concentration, and SiO_2-water with 3% mass fraction has the best comprehensive performance.

Credit authorship contribution statement

Zongpeng Ma: Software, Methodology, Investigation, Writing – original draft, Validation. Ying Huang: Guidance, Financial support. Xiaoling Chen: Language help. Jiangnan Song: Supervision, Writing–review & editing. Xiang Zhang: Supervision, Project administration. Lunjun Chen: translation, Financial support.

Acknowledgment

Authors thank the financial support of the Guizhou Provincial Natural Science Foundation of China (Grant No. [2020]1Y238) and the Introduction of talent research projects of Guizhou University (Grant No. (2018)17) for this paper.

Nomenclature

A – tube cross sectional area, [m^2]
C_p – specific heat, [Jkg^{-1}K^{-1}]
D_h – hydraulic diameter, [mm]
f – friction coefficient, [–]
h – convective heat transfer coefficient, [Wm^{-2}K^{-1}]
k – thermal conductivity, [Wm^{-1}K^{-1}]
L – cross-sectional perimeter, [mm]
m_v – mass-flow, [m^{-3}s^{-1}]
Nu – Nusselt number, [–]
P – pressure, [Pa]
Re – Reynolds number, [–]
S – area of inner tube wall, [m^2]
T – temperature, [K]
u – average fluid velocity, [ms^{-1}]
V – velocity vector, [ms^{-1}]

Greek symbols

μ – dynamic viscosity, [kgm^{-1}s^{-1}]
ρ – density, [kgm^{-3}]
φ – nanoparticle volumetric concentration, [%]
η – comprehensive performance index, [–]
κ – Boltzmann constant, (= 1.381×10^{-23} J/K)

Subscripts

a – atmopshere
in – inlet
out – outlet
ave – average
w – wall
p – particle
nf – nanofluid
bf – base fluid

Superscript

– – average over the tube length

References

[1] Ali, S., Wang, C.-C., Heat Transfer Enhancement in Fin-and-Tube Heat Exchangers–A Review on Different Mechanisms, *Renewable and Sustainable Energy Reviews, 137* (2021), 110470
[2] Elsebay, M., *et al*., Numerical Resizing Study of Al^2O^3 and CuO Nanofluids in the Flat Tubes of a Radiator, *Applied Mathematical Modelling, 40* (2016), 13-14, pp. 6437-6450
[3] Teng, T.-P., *et al*., Evaluation of Heat-Exchange Performance of Carbon-Based Nanofluids for Air-Cooled Exchangers with Different Cross-Section Shapes, *Applied Thermal Eng., 179* (2020), 115725
[4] Morteza, K.-A., Zahra A.-L., Forced Convection In Twisted Minichannel (Tmc) With Different cross section shapes: a numerical study, *Applied Thermal Engineering, 93* (2016), Jan., pp. 101-112
[5] Leong, K. Y., Hwai, C. O., Entropy Generation Analysis of Nanofluids Flow in Various Shapes of Cross Section Ducts, *International Communications in Heat and Mass Transfer, 57* (2014), Oct., pp. 72-78
[6] Horvat, A., *et al*., Comparison of Heat Transfer Conditions in Tube Bundle Cross-Flow for Different Tube Shapes, *International Journal of Heat and Mass Transfer, 49* (2006), 5-6, pp. 1027-1038
[7] Gholami, A., *et al*., Thermal–Hydraulic Performance of Fin-and-Oval Tube Compact Heat Exchangers with Innovative Design of Corrugated Fin Patterns, *International Journal of Heat and Mass Transfer, 106* (2017), Mar., pp. 573-592
[8] Hussein, A. M., *et al*. The Effect of Cross Sectional Area of Tube on Friction Factor and Heat Transfer Nanofluid Turbulent Flow, *Int. Communications in Heat and Mass Transfer, 47* (2013), Oct., pp. 49-55
[9] Tala, J. S., *et al*., Tube Pattern Effect on Thermalhydraulic Characteristics in a Two-Rows Finned-Tube Heat Exchanger, *International Journal of Thermal Sciences,60,* (2012), Oct., pp. 225-235

[10] Chiam, H. W., *et al*., Numerical Study of Nanofluid Heat Transfer for Different Tube Geometries–A Comprehensive Review on Performance, *Int. Comm. in Heat and Mass Tra.*, *86* (2017), Aug., pp. 60-70
[11] Wang, Y., *et al*., Numerical Simulation of Flow and Heat Transfer Characteristics of Nanofluids in Built-In Porous Twisted Tape Tube, *Powder Technology, 392* (2021), Nov., pp. 570-586
[12] Saidur, R., *et al*., A Review on Applications and Challenges of Nanofluids, *Renewable and sustainable energy reviews, 15* (2011), 3, pp. 1646-1668
[13] Daungthongsuk, W., Somchai W., A Critical Review of Convective Heat Transfer of Nanofluids, *Renewable and Sustainable Energy Reviews, 11* (2007), 5, pp. 797-817
[14] Murshed, S. M. Sohel., Patrice, E., A State of the Art Review on Viscosity of Nanofluids, *Renewable and Sustainable Energy Reviews, 76* (2017), Sept., pp. 1134-1152
[15] Kumar, A., *et al*., Heat Transport in Nanofluid Coolant Car Radiator with Louvered Fins, *Powder Technology, 376* (2020), Oct., pp. 631-642
[16] Azmi, W. H., *et al*., Heat Transfer and Friction Factor of Water Based TiO_2 and SiO_2 Nanofluids Under Turbulent Flow in a Tube, *Int. Communications in Heat and Mass Transfer, 59* (2014), Dec., pp. 30-38
[17] Zhao, N., *et al*., Numerical Investigations of Laminar Heat Transfer and Flow Performance of Al_2O_3–Water Nanofluids in a Flat Tube, *Int. J. of Heat and Mass Transfer, 92* (2016), Jan., pp. 268-282
[18] Manca, O., *et al*., A Numerical Study of Nanofluid Forced Convection in Ribbed Channels, *Applied Thermal Engineering, 37* (2012), May, pp. 280-292
[19] Namburu, P. K., *et al*., Numerical Study of Turbulent Flow and Heat Transfer Characteristics of Nanofluids Considering Variable Properties, *Int. J. of Thermal Sciences, 48* (2009), 2, pp. 290-302
[20] Mohammed, H. A., *et al*., Two-Phase Forced Convection of Nanofluids Flow in Circular Tubes Using Convergent and Divergent Conical Rings Inserts, *International Communications in Heat and Mass Transfer, 101* (2019), Feb., pp. 10-20
[21] Kumar, R., Parmanand, K., Thermophysical Analysis of Al_2O_3/CuO Nanofluid in Water/EG Basefluid for Hybrid Louvered Heat Exchanger, *Proceedings of the Institution of Mechanical Engineers, Part C: Journal of Mechanical Engineering Science, 237* (2023), 5, pp. 1229-1243
[22] Kumar, R., *et al*., Thermal Performance of Automobile Radiator Under the Influence of Hybrid Nanofluid, *Materials Today: Proceedings, 76* (2023), Part 2, pp. 251-255
[23] Vajjha, Ravikanth, S., *et al*., Development of New Correlations for the Nusselt Number and the Friction Factor Under Turbulent Flow of Nanofluids in Flat Tubes, *International Journal of Heat and Mass Transfer, 80* (2015), Jan., pp. 353-367
[24] Mirmasoumi, S., Behzadmehr, A., Numerical Study of Laminar Mixed Convection of a Nanofluid in a Horizontal Tube Using Two-Phase Mixture Model, *Applied Thermal Eng., 28* (2008), 7, pp. 717-727
[25] Pak, B. C., Young, I. C., Hydrodynamic and Heat Transfer Study of Dispersed Fluids with Submicron Metallic Oxide Particles, *Experimental Heat Transfer an Int. Journal, 11* (1998), 2, pp. 151-170
[26] Yu, W., Choi, S. U. S., The Role of Interfacial Layers in the Enhanced Thermal Conductivity of Nanofluids: A Renovated Hamilton–Crosser Model, *Journal of Nanoparticle Research, 6* (2004), Apr., pp. 355-361
[27] Wang, X., *et al*., Thermal Conductivity of Nanoparticle-Fluid Mixture, *Journal of Thermophysics and Heat Transfer, 13* (1999), 4, pp. 474-480
[28] Kamyar, A., *et al*., Application of Computational Fluid Dynamics (CFD) for Nanofluids, *International Journal of Heat and Mass Transfer, 55* (2012), 15-16, pp. 4104-4115
[29] Vajjha, Ravikanth, S., *et al*., Development of New Correlations for Convective Heat Transfer and Friction Factor in Turbulent Regime for Nanofluids, *International Journal of Heat and Mass Transfer, 53* (2010), 21-22, pp. 4607-4618
[30] Azmi, W. H., *et al*., Heat Transfer and Friction Factor of Water Based TiO_2 and SiO_2 Nanofluids Under Turbulent Flow in a Tube, *Int. Communications in Heat and Mass Transfer, 59* (2014), Dec., pp. 30-38.
[31] Fotukian, S. M., Nasr Esfahany, M., Experimental Investigation of Turbulent Convective Heat Transfer of Dilute γ-Al_2O_3/Water Nanofluid Inside a Circular Tube, *International Journal of Heat and Fluid Flow, 31* (2010), 4, pp. 606-612

Paper submitted: August 15, 2022
Paper revised: November 15, 2022
Paper accepted: November 22, 2022